3rd Specialty Conference on Disaster Prevention and Mitigation
3e Conférence spécialisée sur la prévention et la mitigation des désastres naturels

Montréal, Québec
May 29 to June 1, 2013 / *29 mai au 1 juin 2013*

Effect of Scaled Distance on the Deflections of Concrete Columns to Near-field Blast Loading: A Numerical Investigation

Lawrence Abladey and Abass Braimah

Abstract: This paper presents an investigation on the effect of scaled distances on deflections of reinforced concrete columns under near-field loading using a numerical modelling technique. An explicit analysis tool, AUTODYN, was utilised in this study for modelling the nonlinear dynamic behaviour of reinforced concrete columns. The RHT and the 4340 steel constitutive models were used in modelling concrete and steel reinforcement respectively. The maximum column deflections occurred at points below the mid-height for blast loading from explosions with scaled distance of less than 1.0. The blast loading on the column was highly nonlinear at scaled distance of 0.25 while uniform at a scaled distance of 1.0.

Keywords: Material model, Numerical simulation, Deflection, Scaled distance

1 Introduction

Recent terrorist attacks on buildings around the world have motivated the study into the behaviour of structures under blast loadings. Many research works published in the literature study the effects of blast loading on reinforced concrete (RC) elements [1, 2 and 3]. However, most of the research is aimed at response of elements such as columns to far-field loading. Also most of the research has focused on numerical simulations and experimental testing of slabs [1, 2 and 3]. Few have investigated the response of RC columns, in particular, to near-field explosions. According to Braimah and Contestabile [15], the probability of a successful terrorists' attack increases with a decrease in amount of explosives used. Thus it is important to understand the effects of small amounts of explosives at close-in distances on RC columns.

The dynamic behaviour of RC columns subjected to blast loading is usually investigated by analytical/numerical simulations or field testing. Field testing using substantial amounts of explosives can, however, be expensive and thus limits the amount of research works involving field explosive testing. The global response of RC columns have been studied by using single-degree-of-freedom (SDOF) techniques [13] while localized response such as scabbing and cratering is analyzed with semi-empirical methods [4]. Numerical methods are used for simulating RC column response to blast loads where the SDOF techniques or semi-empirical methods are not appropriate or give inaccurate results. The numerical methods are capable of modelling a wider range of problems but require specialized expertise and huge computer resources. However, numerical methods have been reported to yield very accurate simulations of experimental results from explosive field testing [4].

One of the widely used numerical modelling tools in blast response analysis is AUTODYN [17], a hydrocode-based computational fluid dynamics program. AUTODYN has built-in material constitutive models and material equations of state needed for simulating blast wave propagation and interaction with structures. The equations of state include Linear, Polynomial, Shock, Ideal gas, Jones-Wilkins-Lee

(JWL) and the PUFF models while examples of constitutive models include Hydrodynamic, Elastic, Brittle, Von Mises and Johnson Cook models. The material constitutive models links the stresses developed in the materials to deformation and internal energy while the equations of state, express the relationships between the pressure (P), density (ρ), specific volume, and specific energy (e). The conservation equations of mass, momentum and energy are coupled with material models to solve problems involving projectile penetration, impacts, and blast events [5, 6, 7 and 8]. The Euler conservation equations of mass, momentum and energy are presented in equations 1, 2 and 3.

Conservation of mass: $$\frac{\partial \rho}{\partial t} + \rho \frac{\partial v_i}{\partial x_i} = 0 \quad (1)$$

Conservation of momentum: $$\rho \frac{\partial v_i}{\partial t} + \rho v_i \frac{\partial v_i}{\partial t} = + \frac{\partial s_{ij}}{\partial x_i} + \rho f_i \quad (2)$$

Conservation of energy: $$\rho \frac{\partial e}{\partial t} + \rho v_i \frac{\partial e}{\partial x_i} = \frac{P}{\rho}\left(\frac{\partial \rho}{\partial t} + v_i \frac{\partial \rho}{\partial x_i}\right) + s_{ij}\epsilon_{ij} \quad (3)$$

Decomposition of stresses: $$\sigma_{ij} = S_{ij} - \epsilon_{ij} P \quad (4)$$

where S_{ij} is the deviatoric stress, ε_{ij} is the strain rate, f_i is the external force, x_i and v_i are the coordinates and the velocities in the computational grid, respectively.

Numerical computations require constitutive models to describe the behaviour of structural members. In an attempt to accurately predict response of structural members, researchers have developed many constitutive material models with varying degrees of complexity and accuracy [4, 5 and 10]. An accurate constitutive model is able to represent the mechanical process of the material under different loading rates and states of stress. Although concrete is a heterogeneous material, it is modelled as a homogenous material because it is impractical to formulate a constitutive model at the meso-scale and involving the major cause of its heterogeneity [9]. Various studies have been conducted over the years to improve the macro-scale models. The complexities of these models have varied over the years. Most concrete models in AUTODYN have been developed with brittle material features such as pressure hardening, strain hardening and strain rate dependency. Stress and strains are treated separately by hydrocodes in volumetric (P, μ) and deviatoric portions (S_{ij}, ε_{ij})) [7].

2 Concrete constitutive models

Some constitutive models developed to predict the behaviour of RC elements are the Johnson and Holmquist (JH) concrete model [9], the Gebbeken and Ruppert (GR) model [16] and Riedel-Hiermaier-Thoma (RHT) model [7]. The JH model was developed in 1993 to give a comprehensive description of concrete under general loading conditions. This model was initially used for brittle materials such as ceramics and later modified for concrete. Concrete is considered to be linear elastic until failure and concrete damage accumulates with increasing load. The material maintains a residual stress state beyond total failure. The yield surface is not smooth over the pressure range for the JH model; rather, the yield surface has a sharp cut-off plane. Furthermore, the JH model is incapable of solving every static and dynamic problem. Although experiments show inelastic deformations and reduced failure strength, these are not exhibited by the JH model [7]. The GR model was developed from the JH model. The GR model included some modifications and enhancements and added a third stress invariant in defining the strength surfaces and a different expression for the yield surfaces. The yield surface for the GR model is smooth over the pressure range as opposed to the JH model. Material damage is taken into account during strain rate enhancement. A hyperbolic function is used to cap the magnitude of the enhancement factor for very high strain rates. The RHT model, an enhanced form of the JH model, was developed by Riedel et al. [7] and takes into account the third invariant and the strain hardening of concrete. The RHT model also includes an independent fracture surface and a rate dependent hydrostatic tensile strength for concrete. The fracture surface facilitates easy modelling of the softening process of the material. The failure surface is defined as:

$$Y_{fail}(p^*, \theta, \dot{\varepsilon}) = Y_c(p^*) \times r_3(\theta) \times F_{rate}(\dot{\varepsilon}) \quad (5)$$

$Y_c(p^*)$ is defined as:

$$Y_c(p^*) = f_c \times \left[A \times \left(p^* - p^*_{spall} \times F_{rate}(\dot{\varepsilon})\right)^N\right] \quad (6)$$

$$p^* = p/f_c \quad (7)$$

$$p^*_{spall} = f_t/f_c \quad (8)$$

where f_c and f_t are the uniaxial compressive and tensile strength of concrete respectively, and the constants A and N are the model parameters. The rate factor $F_{rate}(\dot{\varepsilon})$ denotes the dynamic increase factor of the tensile strength as a function of the strain rate [10].

$$F_{rate}(\dot{\varepsilon}) = \begin{Bmatrix} \left(\frac{\dot{\varepsilon}}{\dot{\varepsilon_o}}\right)^{\alpha} & : \quad P > f'_c, \ \text{for } \dot{\varepsilon_o} = 30 \times 10^{-0} s^{-1} \\ \left(\frac{\dot{\varepsilon}}{\dot{\varepsilon_o}}\right)^{\beta} & : \quad P < f'_c, \ \text{for } \dot{\varepsilon_o} = 3 \times 10^{-6} s^{-1} \end{Bmatrix} \quad (9)$$

Both α and β are the material constants. The deviatoric section has a triangular shape at low pressures and circular shape at high pressures. The concrete material exhibits a brittle behaviour under low pressures and ductile behaviour under high pressures [7, 8 and 9]. A dynamic increase factor (DIF) is used to enhance the material hydrostatic tensile strength. The material strain hardening is accounted for in the RHT model with the introduction of an elastic strength surface ($Y_{elastic}$) as shown in equation (10):

$$Y_{elastic} = Y_{fail}(p^*/F_{elastic}) \times F_{elastic} \times F_{cap}(p) \quad (11)$$

$$F_{cap}(p) = \begin{Bmatrix} 1 & \text{for } p \le p_u = {}^{f_c}/_{3} \\ \sqrt{1 - \left(\frac{p - p_u}{p_o - p_u}\right)^2} & \text{for } p_u < p < p_o \\ 0 & \text{for } p \ge p_o = p_{el} \end{Bmatrix} \quad (12)$$

Where p_o is the upper limit pressure - at this pressure the yield surface intercepts with the hydrostatic axis. p_u is the lower limit pressure - pressure where the uniaxial compression path intercepts with the elastic surface [8]. The model also introduced an independently defined residual strength to describe the strength of the crushed material.

$$Y_{residual} = B \times (p^*)^M \times \frac{[sgn(p^*)+1]}{2} \quad (13)$$

Where the sign function sgn(p*) is defined as:

$$sgn(p^*) = \begin{Bmatrix} 1 & p^* > 0 \\ 0 & p^* = 0 \\ -0 & pp^* < 0 \end{Bmatrix} \quad (14)$$

The loading ($Y_{loading}$) and post loading surfaces ($Y_{fracture}$) are defined as

$$Y_{loading} = Y_{elastic} + \varepsilon_{pl}/\varepsilon_{pl-presoftening} \times (F_{fail} - Y_{elastic}) \quad (15)$$

$$Y_{fracture} = D + Y_{residual} + (1 - D) \times F_{fail} \quad (16)$$

The definition of damage D is shown in equation (17)

$$D = \sum \frac{\Delta\varepsilon_P}{FS(P^*)} \quad (17)$$

$\Delta\varepsilon_P$ is the accumulated plastic strain

$$FS(P^*) = D_1\left(P^* - p^*_{spall}\right)^{D_2} \quad (18)$$

D_1 and D_2 are input parameters. The parameters ε_{pl} and $\varepsilon_{pl\text{-}presoftening}$ are shown in Figure 1.

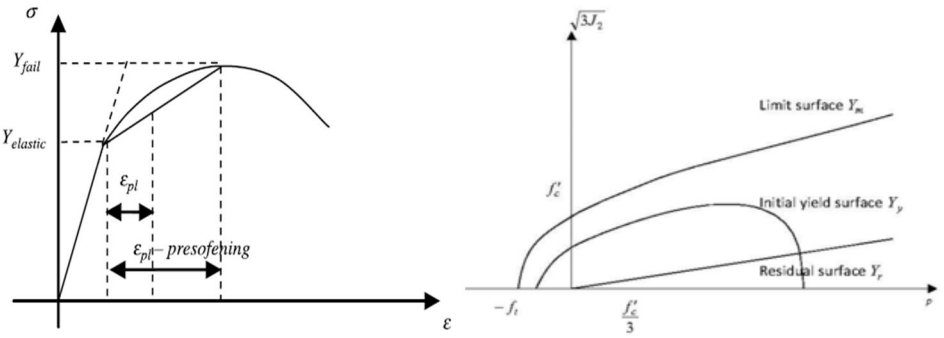

Figure 1- Illustrations of strain hardening and Failure Surface, RHT model [10]

2.1 Explosive properties

Pressures generated in explosions are described using the Jones-Wilkins-Lee equation:

$$p = A_j\left(1 - \frac{w_j}{R_{1j}v_j}\right)^{-j_{1j}v_j} + B_j\left(1 - \frac{w_j}{R_{2j}v_j}\right)^{-j_{2j}v_j} + \frac{w_j E_j}{v_j} \quad (19)$$

Where p is the hydrostatic pressure, v_j is the specific volume E_j is the specific internal energy, A_j, B_j, R_{1j}, R_{2j} and w_j are the material parameters [11].

3 Numerical model

The numerical model used for this research is created using AUTODYN. The model simulates the effects of blast loading on reinforced concrete columns. The explosive charge mass of 100kg ANFO is first modelled as a 2D wedge with an axial symmetry and the results remapped onto the 3D RC column as initial conditions. This technique is used to reduce the computational effort and run time for the problem. The columns have a 300×300 mm cross section and height of 3 m. Figure 2(a) shows the dimensions of the reinforced concrete columns and the reinforcing bars. The diameters of the main bars are 25.2 mm and the diameters of the ties are 11.3 mm with 150 mm tie spacing. The concrete is modelled using a Lagrange grid. Lagrange grids move with the materials, hence no transport of material from element to element occurs. The reinforcing steel bars are modelled using beam elements. The concrete and the reinforcing steel bars were placed in an Euler grid which is used to model both the ANFO explosives and the surrounding air. Euler grids enable material flow through them, which is ideal for modelling fluids and gases. AUTODYN uses a coupled multi solver approach to arrive at solutions. Moreover, these solutions are obtained through the interactions of the solvers. The concrete and the reinforcing bars are rigidly joined at the nodes to enforce bond. Also the fluid-structure interaction between the solid elements and air is achieved through an Euler-Lagrange interaction at the interface of the columns. An outflow boundary condition was set for the Euler grid. Fixed supports were also applied to the top and bottom of the columns and reinforcing bars as shown in Figure 2(b). Figure 2(b) also shows the locations of the three points used in recording the deflections of the columns. Point 1 is at 1 m from the base of the column; points 2 and 3 are also located at 1.5 and 2 m respectively.

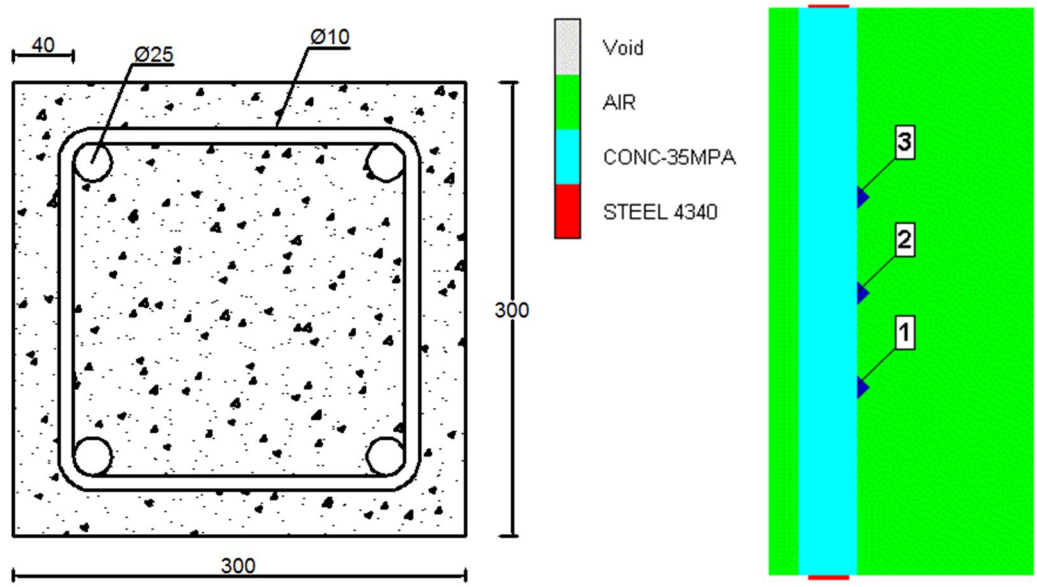

Figure 2. (a) Dimension of concrete column (b) AUTODYN model

The simulation was run for different standoff distances using 100kg ANFO explosive and the columns reinforced with 10M ties at 150 mm spacing. The Three standoff distances are used for this research to determine the effects of standoff distances, in the close-range, on concrete columns. The scaled distances (*Z*) are 0.25, 0.6 and 1; giving corresponding ranges of 1.10, 2.80 and 4.60 m using the relation in equation 20:

$$Z = \left(\frac{R}{W}\right)^{1/3} \quad (20)$$

where *W* is the charge mass in kg and *R* represents the range in metres. The positive phase duration for each standoff distance was calculated using CONWEP and the simulations were run beyond the positive phase duration.

3.1 Material models for numerical setup

The air in the numerical model was modelled using an Ideal gas equation of state (EOS). The relation between the pressures, density, and specific heat are presented in Table 1.

Table 1 Parameters of EOS of air

Reference Density, ρ	1.225 kg/m^3
Specific heat, e	717.6 J/kg
Reference Temperature	288.21 K

Table 2 Parameters of 35 MPa concrete

Parameter	Value	Parameter	Value
Equation of State	P alpha	Thermal Conductivity (J/mKs)	0.00
Reference density (g/cm3)	2.75	Compaction Curve	Standard
Porous density (g/cm3)	2.314	Strength	RHT Concrete
Porous sound speed (m/s)	2.92	Shear Modulus (GPa)	16.70
Initial compaction pressure (kPa)	2.33	Compressive Strength (fc) (MPa)	35.00
Solid compaction pressure (GPa)	6.00	Tensile Strength (ft/fc)	0.10
Compaction exponent	3.00	Shear Strength (fs/fc)	0.18
Solid EOS	Polynomial	Elastic Strength / ft	0.70
Bulk Modulus A1 (GPa)	35.27	Elastic Strength / fc	0.53
Parameter A2 (GPa)	39.58	Failure	RHT Conc.
Parameter A3 (GPa)	9.04	Damage Constant, D1	0.04
Parameter B0	1.22	Damage Constant, D2	1.00
Parameter B1	1.22	Minimum Strain to Failure	0.01
Parameter T1 (GPa)	35.27	Residual Shear Modulus Fraction	0.13
Parameter T2 (kPa)	0.00	Tensile Failure	Hydro (Pmin)
Reference Temperature (K)	295.00	Erosion	Geometric Strain
Specific Heat (J/kgK)	654.00	Erosion Strain	2
		Type of Geometric strain	Instantaneous

The RHT model was used in modelling the concrete while the Steel 4340 constitutive model was used for reinforcing steel bars. The parameters for concrete and reinforcing steel used in the models are presented in Table 2 and Table 3 respectively. A compressive strength of 35MPa was assigned to the concrete material.

Table 3. Steel 4340 parameters

Parameter	Value	Parameter	Value
Equation of State	Linear	Melting Temperature (K)	1793.00
Reference density (g/cm3)	7.83	Strain Rate Constant	0.014
Bulk Modulus (GPa)	159.00	Strain Rate Correction	1st Order
Reference Temperature (K)	300.00	Failure	Principal stress
Specific Heat (J/kgK)	477.00	Principal Tensile Failure Stress (MPa)	600.00
Strength	Johnson Cook	Melting Temperature (K)	1790.00
Shear Modulus (GPa)	77.00	Ref. Strain Rate (/s)	1.00
Yield Stress (MPa)	400.00		

3.2 Validation of numerical model

The AUTODYN numerical model was validated against experimental results from tests conducted by Carriere [14]. Carriere [14] tested RC beams with cross section dimensions of 150×150 mm and length of 2100 mm. The diameter of both the reinforcing bars and ties was 6 mm. Also the tie spacing used in the experiment was 100 mm at mid-span and 50 mm at supports. The beams were subjected to loading from a 15 kg C-4 explosive at 2-m height of burst. Figure 3 shows the concrete failure for both the experimental results and the numerical result. The maximum deflection for the experimental setup is 13 mm as compared to 8 mm for the numerical model. The experimental test has a higher deflection than the AUTODYN model because of differences reflecting surfaces. The AUTODYN model assumed a perfect reflecting surface while in the experiment reflection off the ground surface led to energy transmission into the sand and loss in cratering. Figure 3a represents crack patterns in both the experimental test and numerical analysis and shows very good correlation.

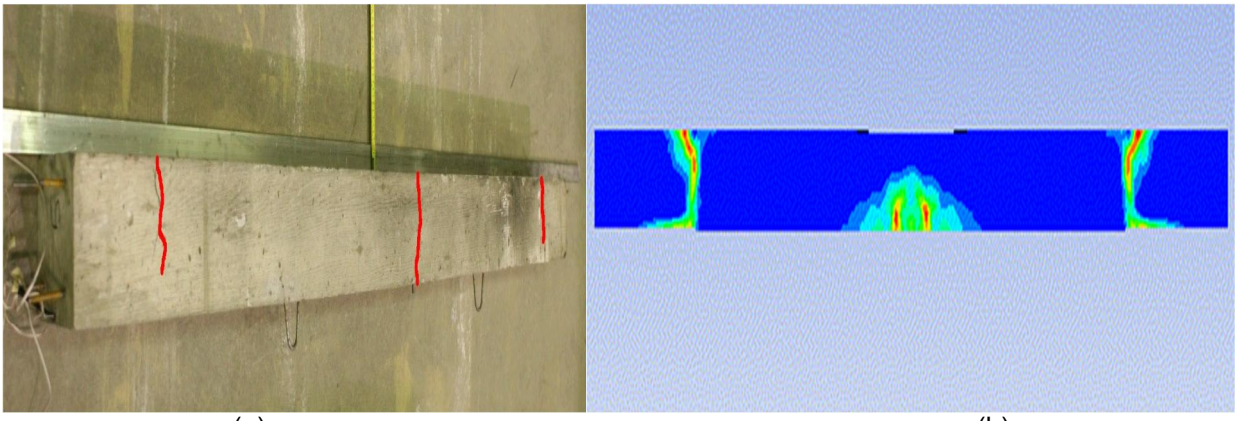

(a) (b)

Figure 3. RC beam failure: (a) Experimental results (b) Numerical results

3.3 Mesh sensitivity analysis

Different mesh sizes were used to investigate the mesh sensitivity of the AUTODYN model. Table 4 shows a summary of the deflections of RC columns and the computational times. The values shown in Table 4 are obtained from running simulations using 100kg ANFO at standoff distance of 0.25 for only 1ms. Mesh 2 was used for the numerical simulation because it gave a high degree of accuracy in terms of deflection without significantly increasing computational cost.

Table 4. Mesh sensitivity analysis summary

mesh number	mesh sizes for all directions (mm)			Deflections (mm)	Computational time (minutes)
	x-direction	y-direction	z-direction		
1	20	15	20	28.4	174
2	15	15	15	29.7	175
3	5	5	5	31	790

4 Results

Figure 4 presents the response of reinforced concrete columns to blast loading from near-field explosion of 100 kg ANFO charge. Three scaled distances of 0.25, 060, and 1.0 were modelled. The figure show severe damage of the concrete column under blast loading in the case of Z=0.25. Damage is concentrated to the lower half of the column (Figure 4(a)). This is expected as the blast loading from near-field explosion is highly nonlinear with highest pressure values at the base of the column from hemispherical blast loading. With increasing scaled distance, standoff distance, the column damage levels decrease (Figure 4(b) and Figure 4(c)).

Table 5 presents a summary of the maximum deflections for three columns at the three scaled distances. The deflections were monitored at three-points along the height of the column. The maximum deflection of the columns with scaled distance of 0.25 and 0.6 occurred at the lower third-point, 1.0 m from the base of the column while for the column with scaled distance of 1.0 the maximum deflection occurred at the mid-height. This is due to the nonlinearity in blast load distribution along the height of the column. For example, using CONWEP to calculate the blast pressure at the deflection monitoring points, the pressure varied by about 54% at the lower third and upper third points, 1.0 m and 2.0 m from the column base respectively for the case with Z = 0.25. Pressure calculation at the same locations for the case with Z=1.0 resulted in a pressure difference of only 16%. Thus, for scaled distances greater than 1.0, the shock front is likely planar resulting in simultaneous and uniform loading of the column face. Figure 5 presents the deflection time history of the columns under blast loading at the three scaled distances. Figure 5(a) show an increasing deflection at the three monitoring points. As the column was severely damaged, maximum deflection was not attained within the analysis time. The 335 mm deflection would result in a support rotation of 18.5^{o} at the lower support. Figure 5(b) and Figure 5(c) present the deflection time history of the columns with scaled distance of 0.6 and 1.0, respectively. The maximum support rotations at the lower support of the columns were 0.7^{o} and 0.3^{o} respectively. The numerical analysis has shown that for scaled distances less than 1, the maximum deflection of the columns is likely to occur below the mid-height. The significance of this finding is that use of single-degree-of-freedom analysis, where only the response of the mid-height is computed, could lead to erroneous results. Also, the support rotations can be significantly underestimated if use is made of the mid-height deflections.

Table 5. Maximum deflections for the three points on the Column.

	height = 1 m		height = 1.5 m		height = 2 m	
z	Max (mm)	Min (mm)	max	min	max	min
0.25	335.0	0.0	183.0	0.0	88.2	0.0
0.6	12.4	-1.0	11.5	-3.6	8.8	-5.5
1.0	6.7	-6.9	8.1	-9.4	7.6	-9.4

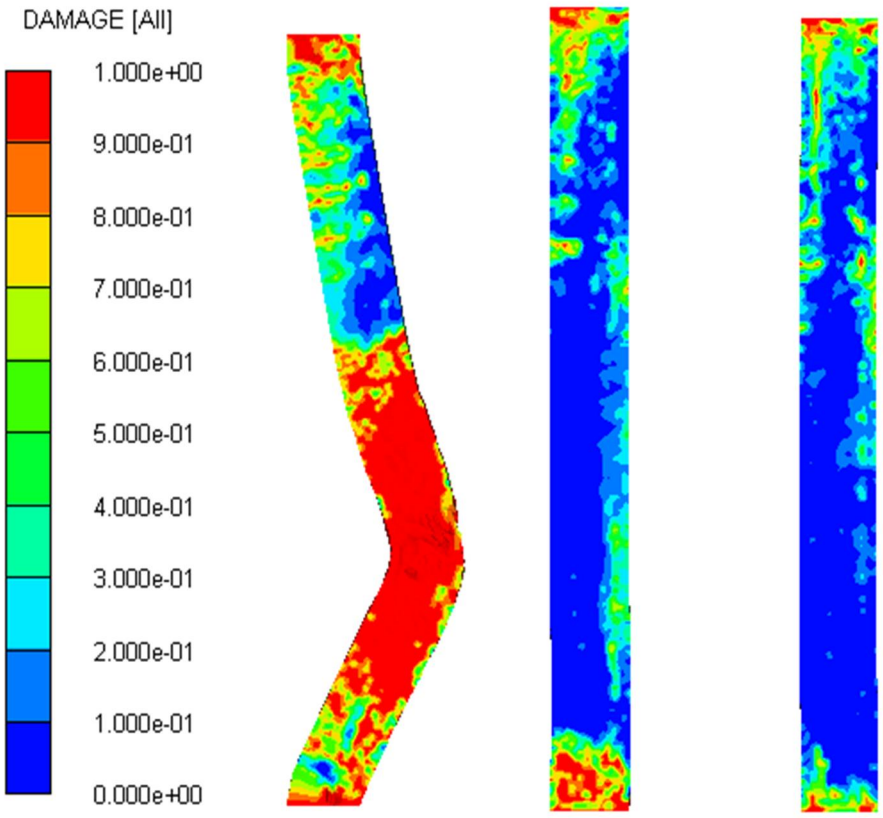

Figure 4. Column damage profile for different stand-off distances: (a) 0.25 (b) 0.6 (c) 1.0

(a)

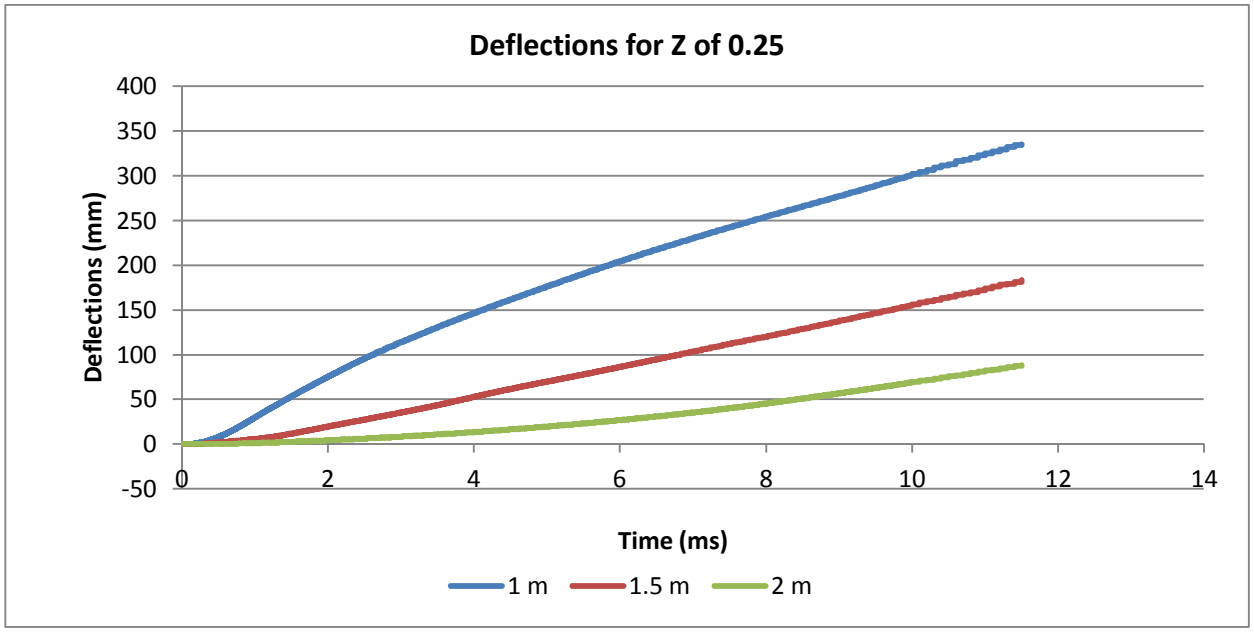

(b)

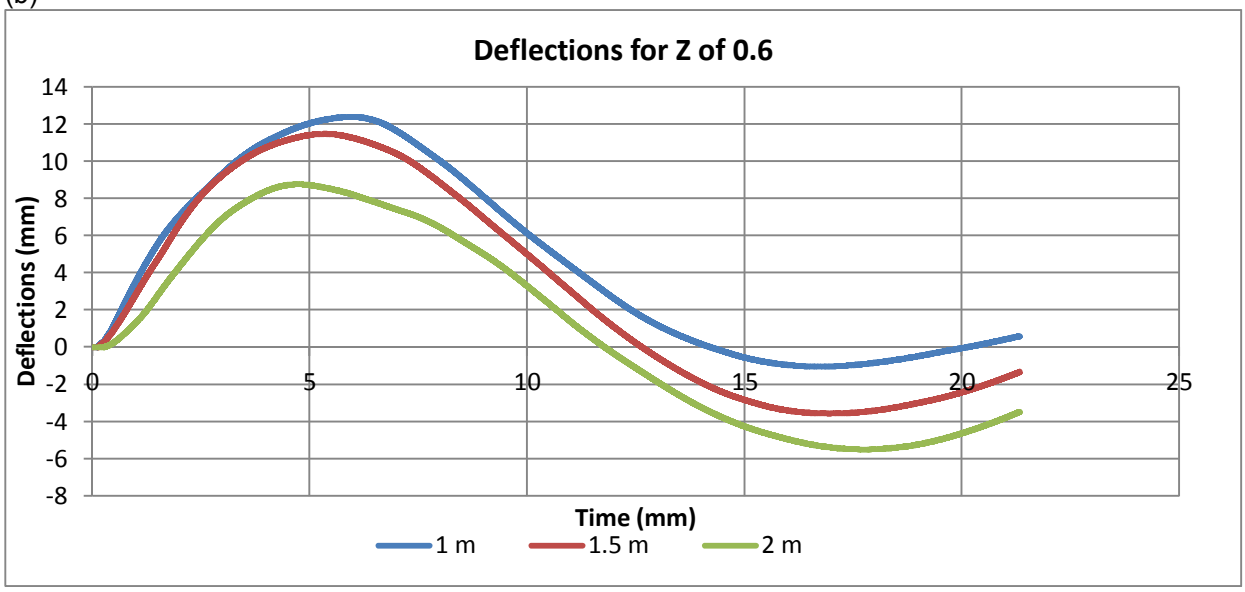

(c)

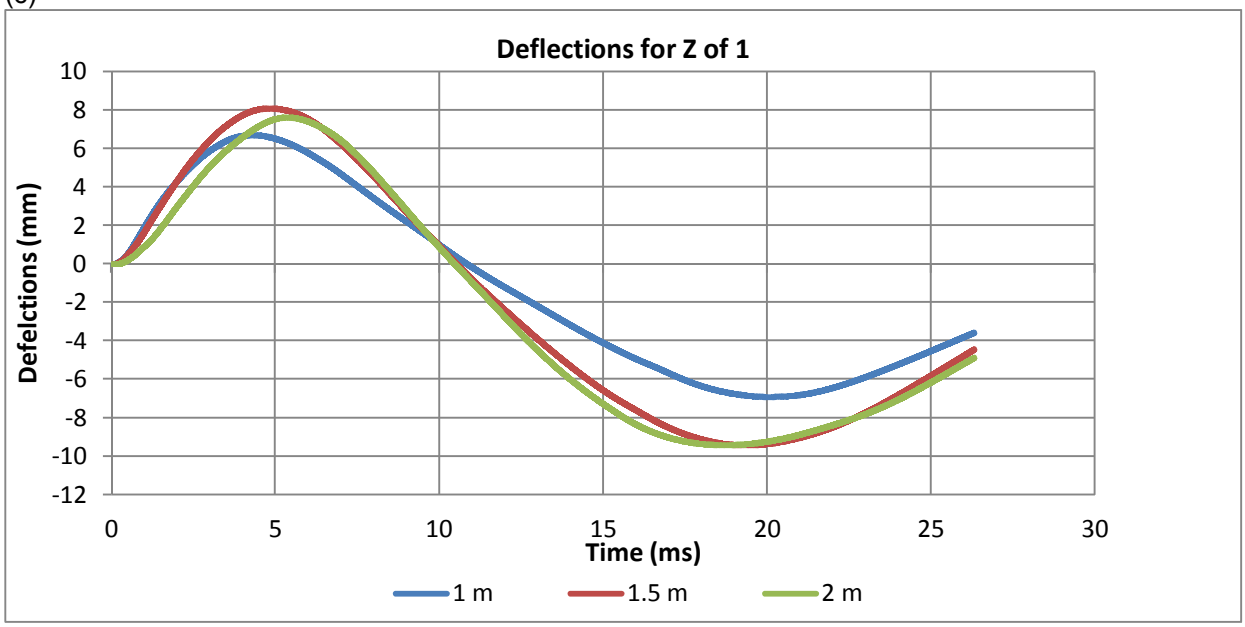

Figure 5. Deflections of columns for different stand-off distances: (a) 0.25 (b) 0.6 (c) 1

5 Conclusions

The response of reinforced concrete columns subjected to near-field explosions was investigated by use of AUTODYN, a computational fluid dynamics software package. A 100-kg ANFO explosive detonation at a scaled distance of 0.25 was found to severely damage a 300×300 mm concrete column. The maximum column deflections occurred at points below the mid-height for blast loading from explosions with scaled distance of less than 1.0

The blast loading on the column was highly nonlinear at scaled distance of 0.25. At a scaled distance of 1.0, the blast loading was much more uniform.

6 References

[1] Gebbeken, N., Greulich, S. and Pietzsch, A. 2001. Performance of Concrete Based Building Materials against Blast and Impact. In Proceedings of the Fib-Symposium on Concrete and Environment, Berlin.

[2] Weerheijm, J., karthaus, W. and Opschoor, G. 1984. The failure mode of layered concrete constructions due to contact charges. 21st DoD Explosions Safety Seminar, Houston, Texas.

[3] Amelsfort, J. 1990. Critical failure of concrete slabs due to contact charges, 24th DoD Explosions Safety Seminar, St. Louis, Missouri.

[4] O'Grady, H., Hayhurst, C., and Fairlie, G. 1996. The Numerical Simulation of Warheads, Impact and Blast Phenomena using AUTODYN-2D and AUTODYN-3D. South African Ballistics Synposium, Stellenbosch, South Africa.

[5] Robertson, N., Hayhurst, C., Fairlie, G. 1994. Numerical simulation of impact and fast transient phenomena using AUTODYN -2D and 3D. Nuclear Engineering and Design, 150(2): 235-241.

[6] Fairlie, G.E. 1997. Efficient analysis of high explosive air blast in complex urban geometries using the AUTODYN-2D & 3D hydrocodes, analytical and experimental methods, 15th Int. In Symposium on the Military Aspects of Blast and Shock, pp. 14-19.

[7] Riedel, W., Thoma, K., Hiermaier, S. and Schmolinske, E. 1999. Penetration of reinforced concrete by BETA-B-500 numerical analysis using a new macroscopic concrete model for hydrocodes. In 9th Int Symp Interaction of the Effects of Munitions with Structures.

[8] Riedel, W., Kawai, N., and Kondo, K. 2009. Numerical assessment for impact strength measurements in concrete materials. International Journal of Impact Engineering, 36(2): 283-293. doi: 10.1016/j.ijimpeng.2007.12.012.

[9] Tu, Z., and Lu, Y. 2009. Evaluation of typical concrete material models used in hydrocodes for high dynamic response simulations. International Journal of Impact Engineering, 36(1): 132-146.

[10] Brannon, R.M., and Leelavanichkul, S. Survey of Four Damage Models for Concrete

[11] Kraus, D., Roetzer, J., and Thoma, K. 1994. Effect of high explosive detonations on concrete structures. Nuclear Engineering and Design, 150(2–3): 309-314. doi: 10.1016/0029-5493(94)90149-X.

[12] Xu Kai and Lu Yong, "Numerical simulation study of spallation in reinforced concrete plates subjected to blast loading." Computers Structures, 2005, 84(5), 431-438.

[13] Zhou X.Q., Kuznetsov V.A., Hao H., Waschl J., “Numerical prediction of concrete slab response to blast loading”, International Journal of Impact Engineering, vol 35(10) 2008,1186-1200.

[14] Carriere, M.D. 2006. Steel reinforced polymer strengthening of reinforced concrete to resist blast loads. In Masters Abstracts International.

[15] Abass Braimah and Ettore Contestabile, Blast Vulnerability Assessment: Challenges and Myths, Structures under Extreme Loading – Proceedings of First International Workshop on Performance, Protection, and Strengthening of Structures under Extreme Loading, August 20-22, 2007

[16] Gebbeken, N. 2000. A new material model for concrete in high-dynamic hydrocode simulations. Archive of Applied Mechanics, 70(7): 463. doi: 10.1007/s004190000079.

[17] AUTODYN, A. 2009. Interactive Non-Linear Dynamic Analysis Software, User’s Manual. SAS IP Inc.